ACS APPLIED MATERIALS & INTERFACES

Research Article

Cite This: ACS Appl. Mater. Interfaces 2020, 12, 3214−3224

www.acsami.org

Switching Anionic and Cationic Semipermeability in Partially Hydrolyzed Polyacrylonitrile: A pH-Tunable Ionic Rectifier

Luthando Tshwenya,[†] Frank Marken,[*,‡] Klaus Mathwig,[§] and Omotayo A. Arotiba[*,†,∥]

[†]Department of Chemical Sciences Formerly known as the Department of Applied Chemistry, University of Johannesburg, Doornfontein 2028, South Africa

[‡]Department of Chemistry, University of Bath, Claverton Down, Bath BA2 7AY, U.K.

[§]Groningen Institute of Pharmacy, Pharmaceutical Analysis, The University of Groningen, P.O. Box 196, AD Groningen 9700, The Netherlands

[∥]Centre for Nanomaterials Science Research, University of Johannesburg, Doornfontein 2028, Johannesburg, South Africa

Supporting Information

ABSTRACT: Membrane materials with semipermeability for anions or for cations are of interest in electrochemical and nanofluidic separation and purification technologies. In this study, partially hydrolyzed polyacrylonitrile (phPAN) is investigated as a pH-switchable anion/cation conductor. When switching from anionic to cationic semipermeability, also the ionic current rectification effect switches for phPAN materials deposited asymmetrically onto a 5, 10, 20, or 40 μm diameter microhole in a 6 μm thick polyethylene-terephthalate (PET) film substrate. Therefore, ionic rectifier behavior can be tuned and used to monitor and characterize semipermeability. Effects of electrolyte type and concentration and pH (relative to the zeta potential at approximately 3.1) are investigated by voltammetry, chronoamperometry, and impedance spectroscopy. A computational model provides good qualitative agreement with the observed electrolyte concentration data. High rectification effects are observed for both cations (pH > 3.1) and anions (pH < 3.1) but only at relatively low ionic strengths.

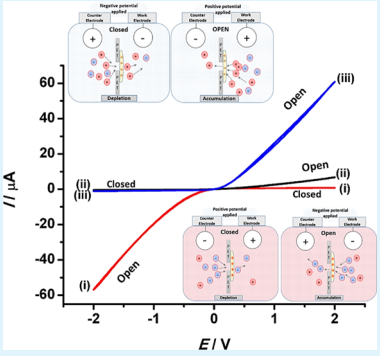

KEYWORDS: *ion channel, membrane, ion gating, double layer, steady state voltammetry, ionic rectifier, polyacrylonitrile*

1. INTRODUCTION

Ionic current rectifiers[1] also known as ionic diodes,[2−5] are membrane-based devices that can selectively allow unidirectional mobility of ions across a membrane (as a result of an applied dc potential difference or as a result of an applied ac polarization). Rectification effects may occur at the microscopic level based on ions interacting with asymmetrically charged nanochannels or nanopores[6−8] or at the macroscopic level based on diffusion−migration phenomena in asymmetric channels and microholes.[9−11] In both cases potential gradient-dependent structural/compositional changes are implicated, and both types of mechanisms, microscopic and macroscopic, may occur in conjunction.[12] The resulting current rectification phenomena are observed as an applied potential-dependent change in impedance (an open state with low impedance and a closed state with high impedance). For macroscopic asymmetric channels, the "open" diode state can be assigned to a situation, where accumulation of the electrolyte lowers the impedance, and the "closed" diode state can be explained with a depletion of the electrolyte.[9] The extent to which an ionic diode rectifies current is typically quantified by the rectification ratio, R_f (i.e., $R_f = |I_+/I_-|$ in which I_+ is the current at a positive potential bias and I_- is the current at the negative potential bias). The higher the rectification ratio, the better the performance of an ionic diode (e.g., for desalination[13]). However, the rectification ratio is potential and condition dependent; it usually increases with higher bias, and it decreases when working against salt gradients.

Research interest in ionic current rectifiers stems in part from the crucial role ion-gated or ion-selective biological membranes play in physiological processes in living organisms.[14] Biological ion channels are known to "open" or "close" to ion transport in response to chemical/redox stimuli or changes in the electric field across the membrane (chemical or voltage gating[15]). Recent progress in this area has been based on materials and devices that mimic such behavior. Nanopore-based diode devices can be fabricated for applicability in areas including biomolecule sensing,[16] single particle detection,[17] controlled drug delivery,[18] energy conversion,[19] and desalination.[20]

Considerable efforts have been made toward the design of current rectifying nanopores or ion channels. Some important examples include "track-etch" membranes[21] and glass capillaries prepared using nanofabrication.[22] The key here is to have asymmetry in charge distribution and/or in the shape of the pores. A combination of a cylindrical microhole [e.g., in a

Received: October 14, 2019
Accepted: December 18, 2019
Published: December 18, 2019

DOI: 10.1021/acsami.9b18583
ACS Appl. Mater. Interfaces 2020, 12, 3214−3224

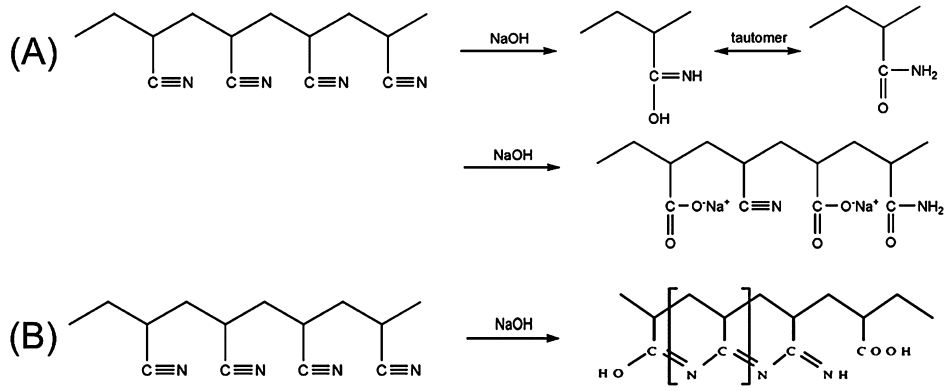

Figure 1. (A) Proposed reaction scheme for the partial hydrolysis of PAN to poly-carboxylate.[41] (B) Proposed reaction scheme for the partial hydrolysis of PAN to conjugated poly-imines.[42]

polyethylene terephthalate (PET) substrate] asymmetrically covered with an ion-conducting semipermeable film results in rectification.[23,24] In this case, asymmetry exist not at the nanoscale but at a macroscopic scale to give rectifier effects. Materials including cellulose,[25] graphene oxide,[9] and ion exchange membranes such as Nafion[26] or Fumasep FKS-30[27] have been investigated. Carbon nanofiber materials applied to a microhole have been shown to produce ionic diode effects and bipolar redox reactions.[28] Under conditions of applied bias and ion migration, some semipermeable materials such as 2D-titania nanosheets[29] also create additional pH gradients because of potential-driven water heterolysis, that occur in regions of highly localized electric fields as a side reaction.

Polyacrylonitrile (PAN) membranes have attracted much attention because of a variety of excellent characteristics, which include thermal stability, tolerance to most solvents, and commercial availability.[30,31] Surface activation processes have been developed to create reactive sites on PAN interfaces for further grafting and/or immobilization.[32,33] Reactive groups on a PAN surface can be generated by UV irradiation,[34] plasma treatment,[35] metal ions activation,[36] or by hydrolysis.[37] Hydrolysis is important as it gives possibilities for further modification. Studies have shown that PAN membranes can maintain their structure and composition when subjected to aqueous acidic conditions. However, in the presence of a base, the nitrile group can be hydrolyzed and converted into carboxyl, acylamide, or amide groups.[38] Possible reaction pathways for NaOH-induced hydrolysis of PAN are indicated Figure 1.[39,40] Note that after mild hydrolysis, both functional groups with a negative charge in alkaline solution (deprotonation of carboxylates) and functional groups with a positive charge in acidic media (protonation of conjugated imines,[41] which are also responsible for a characteristic orange-yellow color[42]) are generated.

It has been reported that partial hydrolysis of PAN renders its surface charged and more hydrophilic, thus greatly improving its interaction ability with aqueous metal ions and with proteins.[39] Here, we exploit the surface charge induced by the partial hydrolysis of PAN and extend its applicability to the development of pH-tunable ionic rectifier materials. We show that films (with a thickness of approximately 13 μm) of partially hydrolyzed polyacrylonitrile (phPAN) asymmetrically covering microholes in PET substrates with a diameter ranging from 5 to 40 μm result in pH responsive ionic diode behavior. The phPAN diodes show positive surface character at a pH below the point of zero charge (which is at approximately pH 3.1), which is attributed to the protonation of nitrogen-containing functional groups. These films conduct anions (thus giving rise to anionic diode behavior). At a higher pH, deprotonation occurs and negative charges are present, which is attributed to carboxylate groups. These films conduct cations (thus giving rise to cationic diode behavior). These diode effects can be switched reversibly from cationic to anionic.

2. EXPERIMENTAL SECTION

2.1. Materials. PAN (M_W 150 000 g/mol), hydrochloric acid (37% v/v), sodium chloride (ACS reagent, >99%), and sodium hydroxide (reagent grade, >98%) were purchased from Sigma-Aldrich (South Africa). Dried *N*,*N*-dimethylformamide (DMF) was purchased from Sisco Research Laboratories Pvt. Ltd. (India). The PET films used for diode fabrication were supplied by Laser Micromachining Limited (St. Asaph, United Kingdom) and contained single microholes (drilled by laser machining) according to specification (diameters of approximately 5, 10, 20, or 40 μm). Ultrapure water (18.2 MΩ cm at 22 °C) was used to make all solutions used.

2.2. Ionic Diode Fabrication. A 10% w/v PAN solution (in DMF) was prepared by dissolving 0.1 g of dry PAN in 1000 μL DMF by first agitating it for 30 min using an ultrasonic bath, followed by stirring for 12 h at room temperature to achieve complete homogeneity. About 5 μL of the homogeneous solution was drop-dried onto a single side of a PET film (placed on glass slide previously coated with 1% w/v agarose gel[26]), where the cylindrical hole is situated, and air dried for 30 min (this ensures good adhesion). Immediately after drying, the PET−PAN assembly was soaked in deionized water and stored in water until further use.

To hydrolyze the PAN film (to give phPAN), the PET with the PAN deposit was immersed in 1 M NaOH at 70 °C for about 20 min. Upon immersion, the color of the PAN film turned from whitish-gray to an intense yellow-orange, indicating a successful hydrolysis[42] (see Figure 2). The phPAN diode was always soaked in deionized water to avoid complete drying and wrinkling of the phPAN film.

2.3. Instrumentation. *2.3.1. Fourier Transform Infrared Spectroscopy.* Functional group analysis was performed on a PerkinElmer Fourier transform infrared (FT-IR) spectrometer using an ATR

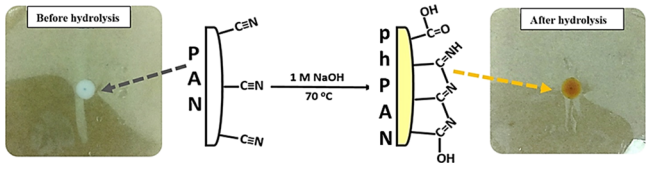

Figure 2. Partial hydrolysis of a PAN film asymmetrically covering a microhole (diameter = 20 μm) on a PET substrate.

DOI: 10.1021/acsami.9b18583
ACS Appl. Mater. Interfaces 2020, 12, 3214−3224

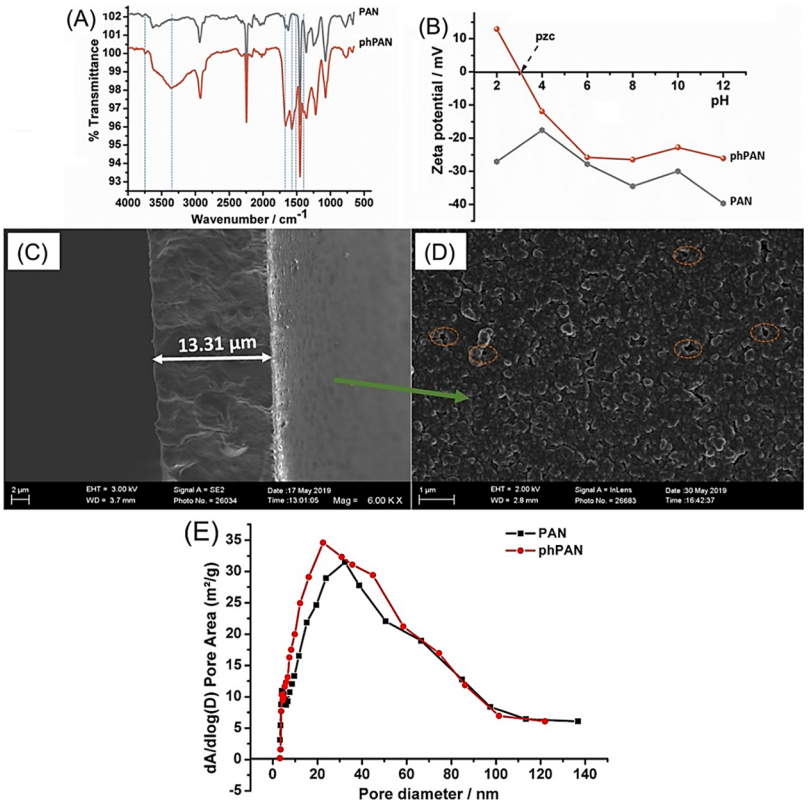

Figure 3. (A) FTIR spectra for PAN and for phPAN. (B) Zeta potential data for PAN and phPAN in aqueous solution (adjusted with HCl or NaOH). (C) Side view scanning electron micrograph showing the thickness and morphology of the phPAN film. (D) Top view micrograph showing the morphology and some pores (encircled) on the phPAN film surface. (E) Data from BET nitrogen adsorption measurements transformed (BJH) into pore diameter distribution for PAN and for partially hydrolyzed PAN.

module. PAN films were hydrolyzed using the procedure described in Section 2.2, allowed to dry completely overnight, crushed, and analyzed using an ATR module. This was contrasted to dry PAN films that were exposed to pure water.

2.3.2. Zeta Potential Measurement. Surface charge analysis for phPAN was studied using a Malvern Zetasizer (South Africa). About 100 mg of PAN was pulverized in order to achieve a uniform and very small particle size, suspended in 1 M NaOH (in a small beaker) and agitated by sonication for 10 min, followed by heating at 70 °C for 20 min using an oven. The yellow phPAN product was filtered and washed a few times with deionized water, followed by drying in air overnight. About 2 mg of the dry phPAN powder was redispersed in ultrapure water adjusted with HCl or NaOH to give different pH values. This measurement was contrasted with pulverized pure PAN.

2.3.3. Scanning Electron Microscopy. Imaging, cross-sectioning, and pore size distribution were studied on a Zeiss Crossbeam 540 FEG SEM coupled with an energy dispersive spectrophotometer detector (Czech Republic), using a 12.7 mm diameter 45/90° chamfer specimen stub, to allow film thickness measurements. This was carried out by depositing a 10% w/v PAN solution (in DMF) onto a glass substrate and suspending the slide in a water bath. After the film detached from the slide, it was transferred to another bath containing 1 M NaOH and was heated for 20 min, followed by washing with deionized water and allowed to dry for an hour. The dry phPAN film was vertically mounted on a carbon-coated chamfer stub, with the film slightly protruding and coated with a thin layer of carbon.

2.3.4. Brunauer–Emmett–Teller Surface Area and Porosity Measurements. A Micromeritics Tristar 2 surface area and porosity analyzer (United States of America) was used to study the surface and pore properties of both PAN and phPAN. To make phPAN, about 200 mg of PAN powder was soaked and heated in 1 M NaOH at 70 °C for ∼30 min (or until PAN changed to a similar orange color as the films used to make the phPAN based ionic diode), followed by washing with deionized water to an almost neutral pH and drying at 60 °C for 12 h using a vacuum oven. Prior to Brunauer–Emmett–Teller (BET) analysis, both samples were degassed with gaseous nitrogen at 120 °C for 12 h prior removing adsorbed water molecules. The measurements were carried out at −196 °C, and pore analysis was performed according to the BJH model.

2.3.5. Electrochemical Studies. The ionic transport properties of the PAN-based ionic diodes were studied by measuring current–voltage (I–V) curves, and chronoamperometry and electrochemical impedance responses using an Ivium CompactStat potentiostat (The Netherlands). A PET film with the hydrolyzed PAN film deposit was mounted between two electrolyte chambers filled with electrolyte solution. The membrane voltage was controlled in a 4-electrode configuration. The phPAN film was always positioned to face the working (WE) and sense electrodes (SE), while the backside of the PET film faced the counter (CE) and reference electrodes (RE). The reference and sense electrodes were identical Ag/AgCl (1 M KCl) electrodes, while the working and counter electrodes were Pt wires. In voltammetry experiments, a potential scan rate of 50 mV s^{-1} was used throughout.

2.3.6. Comsol Simulation. The rectification effect and voltammetric data were modeled by finite element analysis (COMSOL Multiphysics 5.4). Based on our previous numerical model,[43] the Poisson–Nernst–Planck equations were solved to determine the distribution of the potential and cation and anion concentrations of two reservoirs separated by an ionomer membrane connected to a microhole. See the Supporting Information for details on the simulation and geometry. We modeled the phPAN film using a fixed charge density of 60 mM -e^{-}, corresponding to 5.8 kC/dm^3, and a reduced ion diffusivity of 40% of the bulk values for H^+ and Cl^-.

DOI: 10.1021/acsami.9b18583
ACS Appl. Mater. Interfaces 2020, 12, 3214–3224

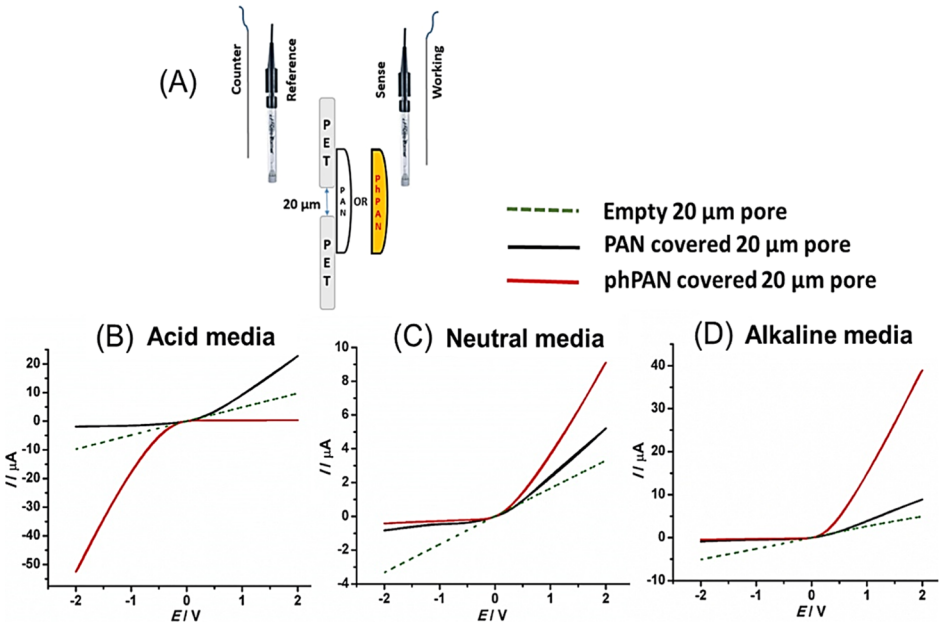

Figure 4. (A) Electrochemical measurement configuration with an asymmetric deposit of PAN or phPAN on a 20 μm diameter microhole in PET. (B) Cyclic voltammograms for an empty 20 μm diameter microhole (green dashed), PAN-covered 20 μm diameter microhole (black solid), and a phPAN-covered microhole (red solid) in 10 mM HCl. (C) As (B) but in 10 mM NaCl. (D) As (B,C) but in 10 mM NaOH.

3. RESULTS AND DISCUSSION

3.1. Characterization of phPAN Films. *3.1.1. Functional Group and Surface Charge Analysis.* To confirm the overall success/extent of the partial hydrolysis, infrared spectroscopy measurements were employed. The spectra of PAN before and after hydrolysis are shown in Figure 3A. Dotted lines indicate new and enhanced absorption bands induced by the partial hydrolysis. Upon hydrolysis, the presence of the broad peak at 3354 cm^{-1} can signify introduction of OH groups to the PAN structure, which might confirm the presence of carboxyl groups. The sharp peak at 2967 cm^{-1} and the shoulder at 2874 cm^{-1} signify the presence of asymmetric and symmetric stretches in CH, CH_2, and CH_3 groups. These are present in both the PAN and phPAN spectra. The sharp peak at 2247 cm^{-1} is a characteristic of C≡N groups present in both PAN and phPAN spectra, which suggests that not all the nitrile groups are converted during the partial hydrolysis process. The peak at 1683 cm^{-1} (C═O stretch) is enhanced in the phPAN spectrum and may be an indication of the conversion of some nitrile groups to amide bonds and carboxyl moieties. The new peaks at 1560, 1397, and 1219 cm^{-1} in phPAN spectra have been reported to indicate the presence of the conjugated imine (−C═N−) sequences.[44] The addition of these functional groups to the film causes color changes (from white to yellow-orange), thereby visually confirming the success of the partial hydrolysis reaction.

Zeta potential measurements were conducted to study the surface charge of PAN and phPAN as a function of pH. PAN was pulverized, and the resulting powder was agitated for 10 min in 1 M NaOH and placed in an oven at 70° for 20 min to achieve partial hydrolysis. The product was filtered, washed with deionized water (until a close to neutral pH was obtained for the filtrate), and then dried. Exactly 2 mg of the resulting phPAN powder was suspended with ultrasound in water at different pH values (ranging from pH 2 to 12). Figure 3B shows that pure PAN material has a negative surface charge throughout the pH range consistent with literature reports.[45] However, upon partial hydrolysis, a net positive surface charge is observed below approximately pH 3.1. Therefore, the point of zero charge (pzc) is approximately at pH 3.1. It will be shown below that such switching behavior at different pH values is important for pH switchable ion conduction/semipermeability, allowing anion conduction at a pH below the pzc (with positive surface charge dominating) and cation conduction at a pH above the pzc (with negative surface charge dominating).

3.1.2. Film Thickness, Porosity, and Surface Morphology. In order to determine the morphology and thickness of the phPAN film, scanning electron microscopy (SEM) imaging and cross-sectioning was employed. Figure 3C shows a side view image of the phPAN film and the film thickness of approximately 13 μm. The top view of the film appears smooth with some irregular pattern, with some evidence for porosity (dotted circular features in Figure 3D). The average diameter of SEM-visible pores is approximately 130 nm. It seems very likely that many smaller pores (not visible by SEM) are present within the structure. Brunauer−Emmett−Teller surface area analysis (BET analysis) for PAN suggests an area of 29.8 ± 0.4 m^2 g^{-1} and for phPAN, the area is 35.0 ± 0.4 m^2 g^{-1}, consistent with low levels of etching or structural change during partial hydrolysis. The pore size distribution (BJH) for both materials is shown in Figure 3E. A typical pore size of 20−30 nm is observed for both materials.

3.2. Electrochemical Characterization of phPAN Films. *3.2.1. Ionic Diode Mechanism.* The geometry of ionic diode in cyclic voltammetry experiments is depicted in Figure 4A. In the absence of PAN or phPAN covering a 20 μm diameter microhole on a 6 μm thick PET substrate, a straight line current−voltage response suggests resistive behavior and no rectification (see dashed line). Straight-line $I-V$ curves indicative of resistance are obtained in acidic, neutral, or in alkaline media. The currents are dominated by the specific resistivity of the aqueous electrolyte solution filling the pore (with diameter = 20 μm and thickness = 6 μm). The slope of

DOI: 10.1021/acsami.9b18583
ACS Appl. Mater. Interfaces 2020, 12, 3214−3224

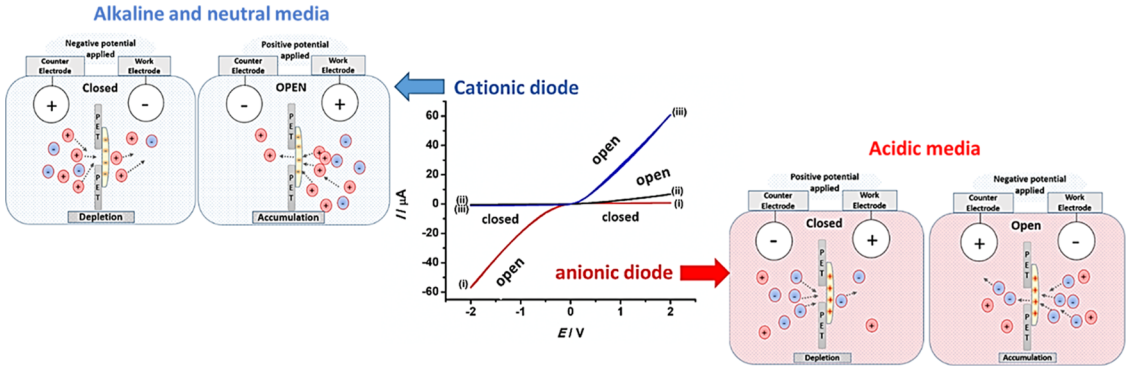

Figure 5. Cyclic voltammetry (scan rate 50 mV s^{-1}) of the phPAN film asymmetrically covering a 20 μm diameter microhole on a PET film substrate in (i) acid media (10 mM HCl on both sides), (ii) neutral media (10 mM NaCl on both sides), and (iii) alkaline media (10 mM NaOH on both sides). Also shown are schematic drawings for the four mechanistic cases of a cationic diode and an anionic diode under positive potential and negative potential polarization.

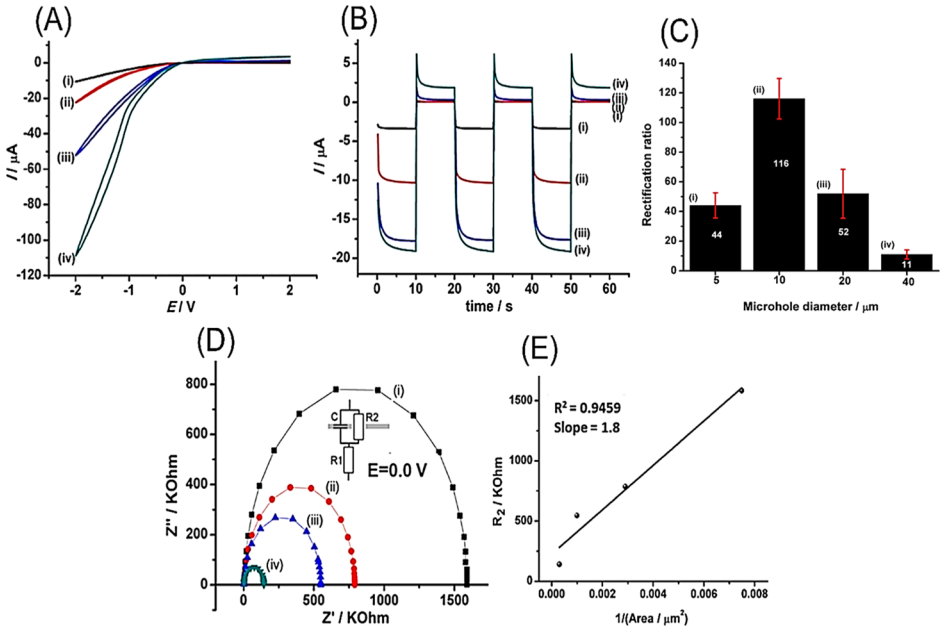

Figure 6. (A) Cyclic voltammograms (scan rate 50 mV s^{-1}) for a phPAN deposit on a (i) 5 (ii) 10, (iii) 20 and (iv) 40 μm diameter microhole in a PET substrate immersed in 10 mM aqueous HCl. (B) Chronoamperometry data for the phPAN diode under the conditions described above. (C) Plot of the rectification ratio (the absolute of the ratio of currents at +1 and at −1 V) vs microhole diameter, error bars are included. (D) Nyquist plots showing the effect of the increasing microhole diameter with bias 0.0 V for a PET substrate immersed in 10 mM aqueous HCl (in the frequency regime 100−0.1 kHz, 100 mV amplitude). (E) Linear plot for diode resistance R_2 as a function 1/area for the different sized microholes.

the $I-V$ curves can be used to calculate the resistivity of the microhole, taking into account both access diffusion and cylindrical hole transport.[46] The resistance was determined to be 205 KΩ in 10 mM HCl, 602 KΩ in 10 mM NaCl, and 389 KΩ in 10 mM NaOH, consistent with the trend in relative specific conductivities for these electrolyte solutions.[47]

When a PAN film asymmetrically covers a microhole (before hydrolysis, see Figure 4), ionic current rectification or cationic diode behavior is observed (consistent with cation semipermeability of PAN). The currents are higher when a positive voltage bias is applied, as compared to when a negative voltage bias is applied. The diode performance or the rectification ratio (calculated as absolute ratio of current −1 V divided by the current at +1 V) for the diode is 5, 3, and 5 in 10 mM HCl, 10 mM NaCl, and 10 mM NaOH, respectively.

After partial hydrolysis, phPAN is obtained and new effects are observed especially in acidic electrolyte (see Figure 4B). The current in the negative potential range is now greatly enhanced ("open diode") and higher than those for both the unmodified PET or for the pure PAN. The currents in the positive potential range are now suppressed ("closed diode") and are lower than those shown for the cases of the open pore or the pure PAN. This effect is indicative of anion conduction or anionic diode behavior and associated with the positive surface charge present on phPAN under acidic conditions below pH 3.1. This positive surface charge or the extent of partial hydrolysis were optimized as a function of hydrolysis time (see supplementary Figure S4 showing $I-V$ curves obtained as a result of varying PAN hydrolysis when exposed to 1 M NaOH at 70 °C, from 5 to 25 min). The best diode behavior was achieved with 20 min hydrolysis. Increasing exposure time longer than this did not improve diode behavior and instead resulted in reduced film stability.

DOI: 10.1021/acsami.9b18583
ACS Appl. Mater. Interfaces 2020, 12, 3214−3224

In aqueous 10 mM HCl (pH approximately 2) based on the zeta potential, the surface of phPAN is positive. This charge can be linked to the protonation of the nitrogen containing functional groups observed in the FT-IR analysis. In neutral and alkaline media, the surface charge of the phPAN diode becomes negative, and thus, the diode switches and conducts cations (see Figure 4C,D). The magnitudes of the currents observed in the open state of the phPAN diode are enhanced when compared to those observed for the PAN diode. Similar currents are seen in acidic and in alkaline media indicative of a similar ability of phPAN to conduct anions (Cl^-) or cations (H^+, Na^+). This is consistent with a similar zeta potential (ca. ±20 mV) in the acidic and in the alkaline pH range and a similar mobility in phPAN for cations and for anions.

Schematic drawings (see Figure 5) are presented to further illustrate the cases of an anionic and cationic diode. In acid media, because of the positive surface charge from the protonation of nitrogen functional groups, mobile anions (Cl^-) are driven through the phPAN film and microhole region by the applied potential. Usually, for an anionic diode, application of a negative potential to the working electrode drives anions through the phPAN film toward the microhole side, causing an increase in electrolyte concentration or accumulation of anions and cations within the microhole region. Therefore, lowering of the resistance or increasing of the current in the negative potential window cause the "open" state of the anionic diode. Application of a positive potential to the working electrode results in the diffusion of anions from bulk solution through the PET microhole toward the phPAN film. Within the microhole region, this results in electrolyte depletion and a higher resistance or a lower current in the positive potential window (the "closed" state of the anionic diode). Further depletion has also been linked to loss of the positive surface character (deprotonation) for anionic diodes that are deprotonated under low electrolyte conditions. In alkaline media, the open state of a cationic (Na^+) diode is experienced in the positive potential bias, associated with electrolyte accumulation as cations are driven into the microhole region by the positive potential.

3.2.2. Effect of the Microhole Diameter. It is interesting to investigate the effects of the microhole diameter (Figure 6) on ionic current rectification for the phPAN diode. When the phPAN diode is immersed in 10 mM HCl solution, it can be observed that the current increases approximately proportionally with the microhole diameter (Figure 6A). For the bigger microhole (40 μm diameter), the current in the open state (in the negative potential range) increases further, possibly due to the increased area of active phPAN covering the hole allowing "over-limiting" convection effects. In the closed state also, a current increase with diameter occurs. Chronoamperometry data (Figure 6B, −1 V for 10 s and +1 V for 10 s) for the phPAN diode under the conditions described above suggest stable currents with the microhole diameter-dependent switching times. The rectification ratio (based on currents at −1 V and +1 V) is plotted in Figure 6C. Increasing the diameter of the microhole from 5 to 10 μm initially increases diode performance to 116 and then causes a deterioration of the rectification effect.

Impedance measurements at 0.0 V applied potential reveal semicircles that are associated with the charging of the PET film (see capacitor C in Table 1), the solution resistance R_1, and the high frequency resistance R_2 for the diode (at a frequency higher than that for rectifier switching and concentration polarization[26]). The Nyquist plots in Figure 6D demonstrate the effect of R_2 in relation to the microhole diameter. A plot of R_2 versus inverse area (Figure 6E) shows a linear trend as expected for a resistive element. A summary of impedance data is included in Table 1, where R_1 is mainly associated with electrolyte resistance and R_2 represents resistance associated with the phPAN-covered microhole.

Table 1. Summary of EIS Data for the phPAN Diode on Different Sized Microholes, When 0.0 V is Applied in the Frequency Range 100−0.1 kHz, the Amplitude is 100 mV[a]

microhole diameter/μm	R_1/kΩ	R_2/kΩ	C/nF
5	7.2	1583	0.6
10	5.1	785	0.6
20	3.5	546	0.5
40	2.9	140	0.6

[a]Only the high frequency semicircular part of the Nyquist data is analyzed. Although data fits are excellent, device-to-device variations are typically ±30% mainly due to variation in phPAN film properties.

3.2.3. Effect of Ionic Strength. The effect of electrolyte concentration was studied by systematically varying the concentration of aqueous HCl and NaOH from 10 to 500 mM for a phPAN diode (PET film with a 20 μm diameter microhole). Unless otherwise stated, the two compartments of the electrochemical cell were filled with electrolyte solution of the same concentration, and the working and sense electrodes faced the phPAN film.

Figure 7A shows experimental $I-V$ data demonstrating the effect of increasing ionic strength of HCl. Both open and closed state currents increase with electrolyte concentration. As seen from the inset, the open current at −2 V increases approximately linearly with the square root of the concentration of HCl. Derivative plots (Figure 7B) are provided to show more clearly the effect of applied potential on conductivity. At a negative applied potential, a high conductivity is observed, and at positive applied potentials, the conductivity is low. The switch from open to closed occurs mainly in the range from −0.5 to +0.5 V. Figure 7C shows typical open/closed transients when switching the applied potential between −1.0 and +1.0 V. The plateau currents obtained in this way were used to evaluate rectification ratios (see Figure 7D). The rectification ratio is high when the ionic strength is low, and it decreases with an increase in ionic strength. This behavior can be attributed to gradual loss of semipermeability.

A numerical simulation approach can be employed to confirm the mechanism by which the increase in electrolyte concentration affects the ionic diode performance (see Experimental Section). Numerical $I-V$ curves (dashed curves, Figure 7A) show good qualitative and quantitative agreement with experimental values (compare Figures 7A). With increasing electrolyte concentration, the simulated open diode current increases from −17 μA for 10 mM HCl to 216 μA for a 500 mM HCl concentration (at −1 V; note that experimental data were measured up to −2 V), while the rectification ratio continuously decreases with increasing concentrations. To achieve a high rectification ratio, the density of fixed ionomer charges in phPAN (here 60 mM $-e^-$ in the simulation) has to exceed the bulk electrolyte concentration. Therefore, an increase in bulk electrolyte concentration diminishes the rectification effect. Simulated rectification ratios are presented in Figure 7D.

DOI: 10.1021/acsami.9b18583
ACS Appl. Mater. Interfaces 2020, 12, 3214−3224

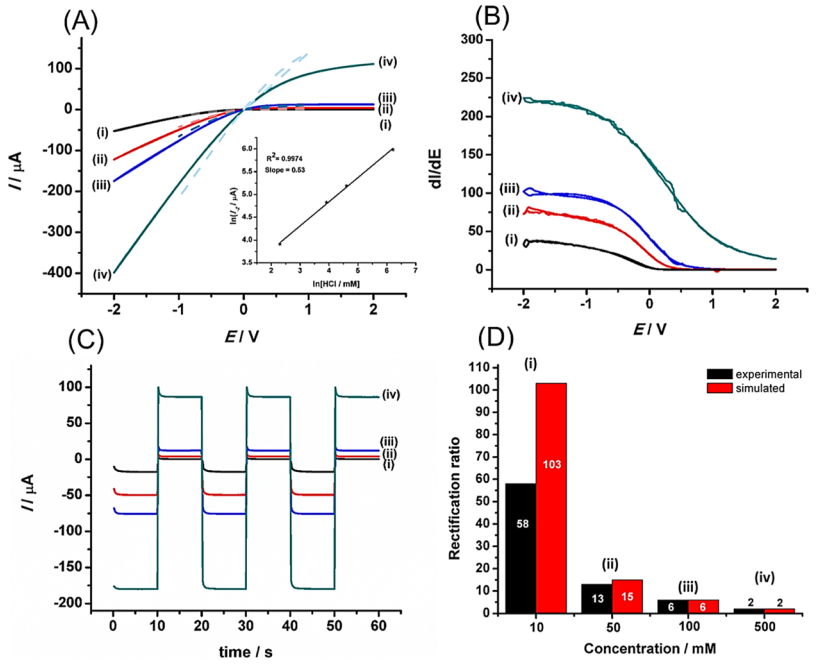

Figure 7. (A) Cyclic voltammograms (50 mV s^{-1}) for a phPAN film asymmetrically covering a PET film with a 20 μm cylindrical hole (phPAN diode) immersed in HCl concentration of (i) 10, (ii) 50, (iii) 100, and (iv) 500 mM on both sides of the PET film. The dashed lines represent simulated $I-V$ curves for a 20 μm cylindrical hole (for similar conditions as described above) and between ±1 V (inset: plot showing a linear increase in current at −2 V vs concentration). (B) Plot of the first derivative of the cyclic voltammograms above. (C) Chronoamperometry data for the phPAN diode under the conditions described above. (D) Bar plot (black) of the rectification ratio (the absolute of the current at −1 V divided by the current at +1 V) vs concentration as obtained from the chronoamperometry data. The corresponding rectification ratios from computer simulations (red) were evaluated at −1 V vs +1 V.

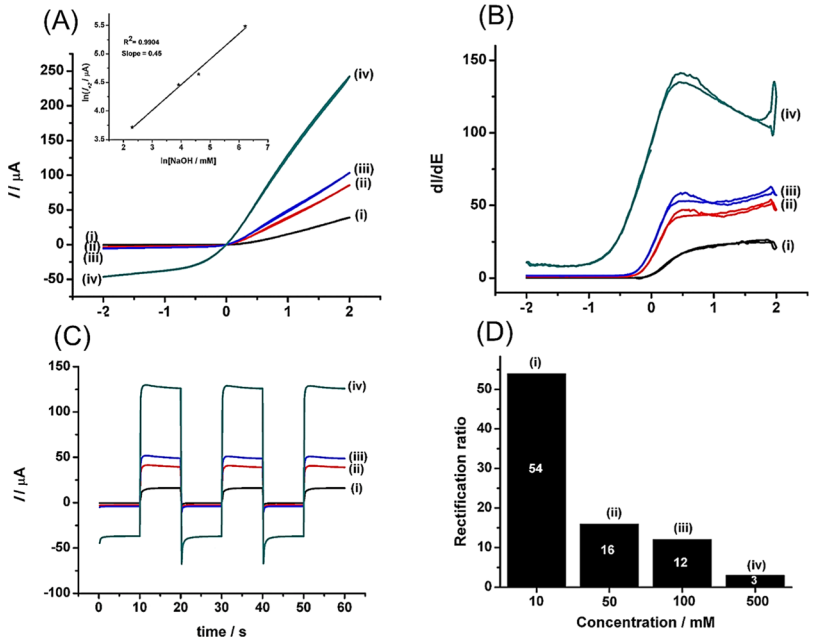

Figure 8. (A) Cyclic voltammograms (50 mV s^{-1}) for a phPAN film asymmetrically covering a PET film with a 20 μm diameter cylindrical microhole (phPAN diode) immersed in NaOH concentration of (i) 10, (ii) 50, (iii) 100, and (iv) 500 mM on both sides of the PET film (an inset showing a linear increase in current at +2 V vs concentration is included). (B) Plot of the first derivative of cyclic voltammograms above. (C) Chronoamperometry data for the phPAN diode under the conditions described above. (D) Plot of the rectification ratio (the absolute of the current at −1 V divided by the current at +1 V as obtained from the chronoamperometry plots vs concentration).

Next, Figure 8A–D shows a summary of experimental data for different sodium hydroxide concentrations. Figure 8A shows $I-V$ curves, which clearly show a gradual increase in open state currents because of increased electrolyte concentration on the phPAN diode. The inset shows linearity in currents at +2 V versus square root of electrolyte concentration. The first derivative of voltammetric data (Figure 8B) shows a switch from low conductivity in the

DOI: 10.1021/acsami.9b18583
ACS Appl. Mater. Interfaces 2020, 12, 3214−3224

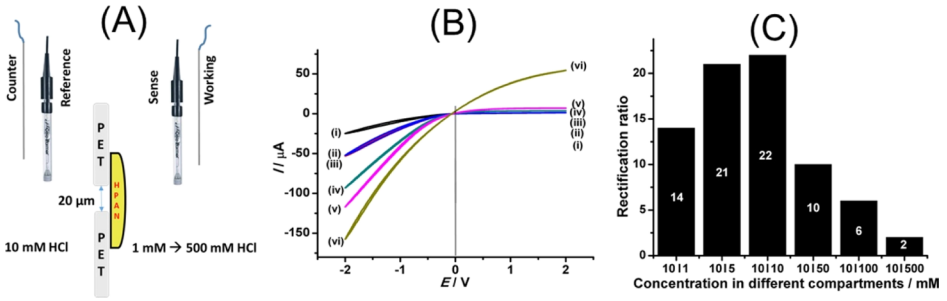

Figure 9. (A) Electrochemical configuration showing how concentration was varied in the working electrode compartment. (B) Cyclic voltammograms (scan rate 50 mV s^{-1}) with 10 mM HCl in the counter electrode compartment and different concentrations from (i) 1, (ii) 5, (iii) 10, (iv) 50, (v) 100, and (vi) 500 mM HCl in the working electrode compartment. (C) Plot of the rectification ratio vs HCl concentration.

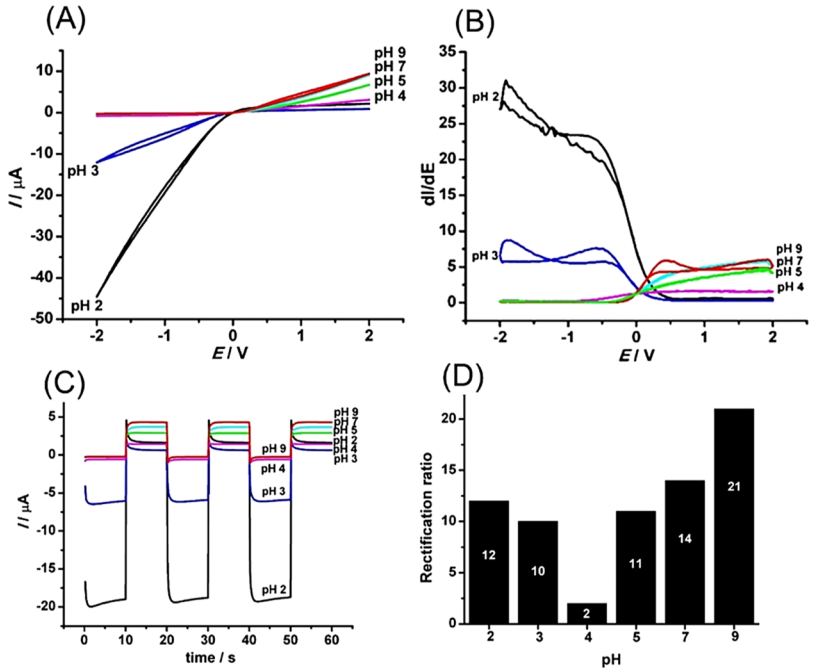

Figure 10. (A) Cyclic voltammograms (50 mV s^{-1}) for a phPAN diode in 10 mM NaCl at different pH values (adjusted with 1 M HCl or NaOH). (B) First derivative cyclic voltammograms. (C) Chronoamperometry data (+1 and −1 V) for 10 mM NaCl at different pH values. (D) Bar graph showing the rectification ratio (absolute ratio of open current/closed current at ±1 V) for the phPAN diode as a function of pH.

negative potential range to higher conductivity in the positive potential range. Chronoamperometry data (Figure 8C) demonstrate the diode switching and a plot of rectification ratios as a function of NaOH concentration is shown in Figure 8D. Again, a loss of rectification occurs with higher electrolyte concentration.

Data for varying the aqueous electrolyte concentration in the working electrode compartment are shown in Figure 9. The concentration of HCl in the half-cell facing the phPAN film was varied from (i) 1, (ii) 5, (iii) 10, (iv) 50, (v) 100, to (vi) 500 mM, while keeping the concentration HCl in the counter electrode compartment constant at 10 mM. This experiment demonstrates ion transport down/up in concentration gradients, via the nanopores or nanochannels present in phPAN. A slight shift in the zero-current potential can be attributed in part to osmotic pressure effects that represent themselves as trans-membrane or Donnan potentials[48] (see Figure 9B). An increase in ionic current with increased concentration is observed corresponding to enhanced conductivity. The rectification ratio is at the highest when equal concentrations (10 mM HCl I 10 mM HCl) fill the two compartments of the electrochemical cell. At lower HCl concentration in the working electrode compartment, the diode has to work against the salt gradient. At higher HCl concentrations, a loss of the rectification ratio due to loss of semi-permeability is likely.

3.2.4. Effect of pH on Cationic and Anionic Semi-permeability. Cyclic voltammetry experiments (see Figure 10) show that pH strongly influences ion conduction and thus ionic current rectification. Qualitatively, the data shows that low pH values <3 clearly promote anion selectivity or semi-permeability, as high ionic currents are observed under a negative potential bias. Adjusting the pH > 4 results in a diode polarity reversal. These results correlate with zeta potential studies. The pH where the net surface charge of the phPAN material is close to zero (the pzc) is close to pH 3.1. This is represented in the rectification data shown in Figure 10C,D.

3.2.5. Effects of Varying Electrolyte Anions or Cations. Figure 11A shows *I*−*V* curves for an asymmetrically deposited phPAN film in aqueous 10 mM acids for HCl, HNO_3, H_2SO_4, and H_3PO_4. In all cases, anionic diode effects are observed. Although chloride, nitrate, and HSO_4^- appear to produce very

DOI: 10.1021/acsami.9b18583
ACS Appl. Mater. Interfaces 2020, 12, 3214−3224

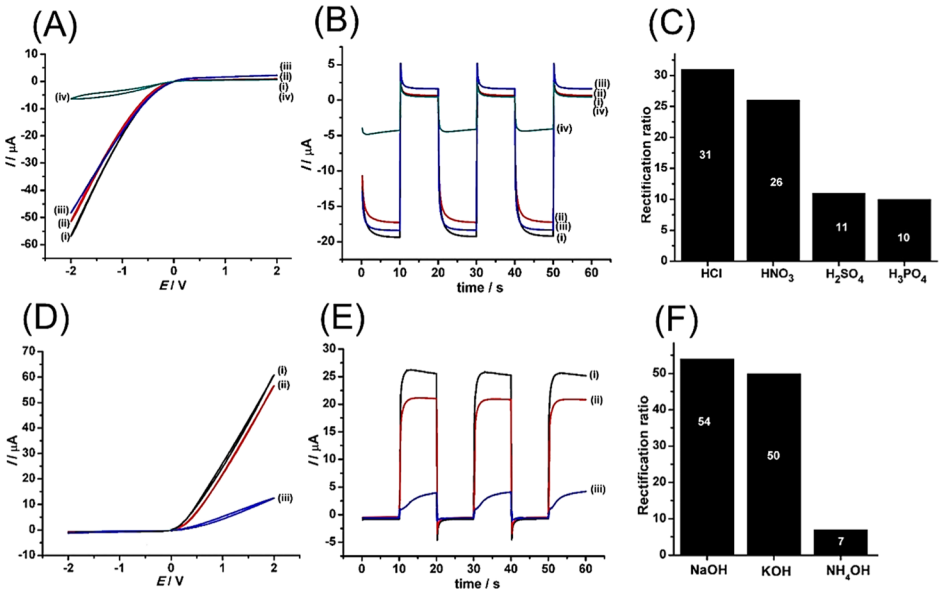

Figure 11. (A) Cyclic voltammograms (scan rate 50 mV s^{-1}) showing the effect of different acidic electrolytes: (i) 10 mM HCl, (ii) 10 mM HNO_3, (iii) 10 mM H_2SO_4, and 10 mM H_3PO_4 filling both compartments (phPAN asymmetrically deposited on a 20 μm diameter microhole). (B) Chrono-amperometry data (−1 and +1 V). (C) Bar graph with rectification ratio data for different acidic electrolytes. (D) As A but for (i) 10 mM NaOH, (ii) 10 mM KOH, and (iii) 10 mM NH_4OH. (E) Same as (B) but for different bases. (F) Same as (C) but for the different bases.

similar characteristics, data for phosphate anions suggest significant changes. In particular, currents in the open state of the diodes are low. The trends in current are confirmed in the chronoamperometry data in Figure 11B. The bar graph of the rectification ratio versus type of acid reveals lower rectification for sulfate and phosphate. These two anions will be present in the form of HSO_4^- and $H_2PO_4^-$, which could suggest that protons play a part in this mechanism. Proton mobility within phPAN could be high compared to that for these anions, and therefore, species such as SO_4^{2-} and HPO_4^{2-} may be formed transiently to significantly slow down ion transport in phPAN pores and lower the rectification ratio.

A comparison of the diode characteristics for 10 mM NaOH, 10 mM KOH, and 10 mM NH_4OH is shown in Figure 11D. Voltammetry and chronoamperometry data show very similar behavior for NaOH and KOH. A slightly lower current for K^+ may be attributed to lower mobility. For NH_4^+ cations, a dramatic change in behavior is observed. Transient formation of protons within the phPAN material could be contributing to a higher resistance and loss of rectification.

The resistance of the phPAN membrane to ion flow at 0 V applied potential can be probed by electrochemical impedance spectroscopy. Data are summarized in Table 2. A single semicircle in the Nyquist plot is interpreted here in terms of R_1, solution resistance, C, PET surface charging, and R_2, the phPAN film resistance combined with the microhole resistance (at high frequency). The R_2 values present an insight into the conductivity under high frequency conditions (higher than the diode switching rate), which may contrast to the dc or low frequency behavior. For the alkaline electrolyte solutions, the trend clearly confirms an increase in resistivity from Na^+ to K^+ to NH_4^+. However, for the acidic solutions, the R_2 value for HCl appears unusually high. The reason for this is currently not clear.

Table 2. Summary of EIS Data for the phPAN Diode (20 μm Diameter Microhole PET Substrate) Exposed to Different Acids and Bases, When 0.0 V is Applied in the Frequency Range 100−0.1 KHz, Amplitude is 100 mV[a]

electrolyte	R_1/KΩ	R_2/KΩ	C/nF
Acidic Solution			
HCl	2.5	539	0.5
HNO_3	2.1	262	0.5
H_2SO_4	1.6	148	0.5
H_3PO_4	4.4	462	0.5
Alkaline Solution			
NaOH	1.5	152	0.5
KOH	3.1	245	0.5
NH_4OH	2.6	1377	0.5

[a]Only the high frequency semicircular part of the Nyquist data is analyzed. Device-to-device variation and errors are estimated to be ±30%.

4. CONCLUSIONS

It has been shown that phPAN as a semipermeable material offers attractive properties because of the ability to act as both cation conductor in alkaline environments and anion conductor in acidic environments. Surface functionalities in microscopic channels in the material are responsible for this change. Both the anion and cation conductors exhibit semipermeability and therefore allow ionic rectifiers/diodes to be formed by asymmetric phPAN deposition onto a thin PET substrate with a microhole. Both, cationic diodes and anionic diodes, are obtained with similar properties and ability to rectify ionic currents. The pzc of the phPAN material has been shown to be linked to the point of the polarity change from anionic to cationic diode. A numerical simulation tool can be employed to rationalize and predict diode behavior, but experimental factors such as imperfection in geometry and additional convective effects (in the overlimiting region) on

DOI: 10.1021/acsami.9b18583
ACS Appl. Mater. Interfaces 2020, 12, 3214−3224

currents currently prevent a quantitative fit of simulation to experimental data.

As a material for ionic diodes, phPAN offers a chemically robust low-cost option, although long term applications, for example, in desalination still need to be developed. Compared to other types of semipermeable materials, phPAN could be useful also when further modified by surface functionalization. Ionic diode performance is linked to charge density, charge mobility, and the degree of semipermeability. All of these parameters will need further optimization without loss of chemical and mechanical robustness under conditions of ac-voltage driven ion transport.

In the future, a wider range of materials with semipermeable properties can be employed for ionic current rectifiers and for applications such as desalination or sensing. The ability of the ionic diode to respond to the environment is shown here for the pH parameter, but similar responses will be possible also for other types of parameters (e.g., heavy metal cation concentration). The ionic diode could be activated by or used to indicate the presence of pollutants, or it could be used to selectively remove cationic or anionic pollutants. By combining several ionic diodes into circuits with more complex behavior, further opportunities arise, for example, for net transport of neutral species or for controlled release of drugs.

■ ASSOCIATED CONTENT

Supporting Information

The Supporting Information is available free of charge at https://pubs.acs.org/doi/10.1021/acsami.9b18583.

Simulation geometry for numerical calculation and boundary conditions; cation, anion and potential distribution; and cyclic voltammetry of a polyacrylonitrile film (PDF)

■ AUTHOR INFORMATION

Corresponding Authors

*E-mail: fm202@bath.ac.uk (F.M.).
*E-mail: oarotiba@uj.ac.za (O.A.A.).

ORCID

Frank Marken: 0000-0003-3177-4562
Klaus Mathwig: 0000-0002-8532-8173
Omotayo A. Arotiba: 0000-0002-8227-8684

Notes

The authors declare no competing financial interest.

■ ACKNOWLEDGMENTS

L.T. thanks the Global Excellence and Stature, University of Johannesburg for Doctoral Scholarship. DST/Mintek Nanotechnology Innovation Centre, University of Johannesburg, South Africa; the Water Research Commission, (grant number: K5/2567) South Africa; the National Research Foundation (CPRR grant numbers: 98887 and 118546), South Africa are acknowledged for their financial support. We thank Dr. Kyle C. Smith (University of Illinois) for helpful discussions.

■ REFERENCES

(1) Lovrecek, B.; Despic, A.; Bockris, J. O. M. Electrolytic Junctions with Rectifying Properties. *J. Phys. Chem.* **1959**, *63*, 750−751.
(2) Guo, W.; Tian, Y.; Jiang, L. Asymmetric Ion Transport through Ion-channel-mimetic Solid-state Nanopores. *Acc. Chem. Res.* **2013**, *46*, 2834−2846.
(3) Chun, H.; Chung, T. D. Iontronics. *Annu. Rev. Anal. Chem.* **2015**, *8*, 441−462.
(4) Guan, W.; Li, S. X.; Reed, M. A. Voltage Gated Ion and Molecule Transport in Engineered Nanochannels: Theory, Fabrication and Applications. *Nanotechnol* **2014**, *25*, 122001.
(5) Koo, H.-J.; Velev, O. D. Ionic Current Devices - Recent Progress in the Merging of Electronic, Microfluidic, and Biomimetic Structures. *Biomicrofluidics* **2013**, *7*, 031501.
(6) Lan, W.-J.; Edwards, M. A.; Luo, L.; Perera, R. T.; Wu, X.; Martin, C. R.; White, H. S. Voltage-Rectified Current and Fluid Flow in Conical Nanopores. *Acc. Chem. Res.* **2016**, *49*, 2605−2613.
(7) Chen, L.-J.; Guo, L. J. Nanofluidic Diodes. *Chem. Soc. Rev.* **2010**, *39*, 923−938.
(8) Zhang, H.; Tian, Y.; Jiang, L. Fundamental Studies and Practical Applications of Bio-inspired Smart Solid-state Nanopores and Nanochannels. *Nano Today* **2016**, *11*, 61−81.
(9) Putra, B. R.; Aoki, K. J.; Chen, J.; Marken, F. Cationic Rectifier Based on a Graphene Oxide-Covered Microhole: Theory and Experiment. *Langmuir* **2019**, *35*, 2055−2065.
(10) Park, S.; Yossifon, G. Electrothermal Based Active Control of Ion Transport in a Microfluidic Device with an Ion-permselective Membrane. *Nanoscale* **2018**, *10*, 11633−11641.
(11) Park, S.; Yossifon, G. Induced-charge Electrokinetics, Bipolar Current, and Concentration Polarization in a Microchannel-Nafion-Membrane System. *Phys. Rev. E* **2016**, *93*, 062614.
(12) Green, Y.; Park, S.; Yossifon, G. Bridging the Gap between an Isolated Nanochannel and a Communicating Multipore Heterogeneous Membrane. *Phys. Rev. E* **2015**, *91*, 011002.
(13) Madrid, E.; Cottis, P.; Rong, Y.; Rogers, A. T.; Stone, J. M.; Malpass-Evans, R.; Carta, M.; McKeown, N. B.; Marken, F. Water Desalination Concept Using an Ionic Rectifier Based on a Polymer of Intrinsic Microporosity (PIM). *J. Mater. Chem. A* **2015**, *3*, 15849−15853.
(14) Huang, X.; Kong, X.-Y.; Wen, L.; Jiang, L. Bioinspired Ionic Diodes: From Unipolar to Bipolar. *Adv. Funct. Mater.* **2018**, *28*, 1801079.
(15) Laucirica, G.; Marmisollé, W. A.; Toimil-Molares, M. E.; Trautmann, C.; Azzaroni, O. Redox-Driven Reversible Gating of Solid-State Nanochannels. *ACS Appl. Mater. Interfaces* **2019**, *11*, 30001−30009.
(16) Howorka, S.; Siwy, Z. Nanopore Analytics: Sensing of Single Molecules. *Chem. Soc. Rev.* **2009**, *38*, 2360−2384.
(17) Harms, Z. D.; Haywood, D. G.; Kneller, A. R.; Jacobson, S. C. Conductivity-based Detection Techniques in Nanofluidic Devices. *Analyst* **2015**, *140*, 4779−4791.
(18) Li, Z.; Yu, L.; Yang, T.; Chen, Y. Theranostic Nanomedicine by Surface Nanopore Engineering. *Sci. China: Chem.* **2018**, *61*, 1243−1260.
(19) Zhu, Z.; Wang, D.; Tian, Y.; Jiang, L. Ion/Molecule Transportation in Nanopores and Nanochannels: From Critical Principles to Diverse Functions. *J. Am. Chem. Soc.* **2019**, *141*, 8658−8669.
(20) Wu, K.; Chen, Z.; Li, J.; Xu, J.; Wang, K.; Li, R.; Wang, S.; Dong, X. Ultrahigh Water Flow Enhancement by Optimizing Nanopore Chemistry and Geometry. *Langmuir* **2019**, *35*, 8867−8873.
(21) Siwy, Z.; Gu, Y.; Spohr, H. A.; Baur, D.; Wolf-Reber, A.; Spohr, R.; Apel, P.; Korchev, Y. E. Rectification and Voltage Gating of Ion Currents in a Nanofabricated Pore. *Europhys. Lett.* **2002**, *60*, 349−355.
(22) Bafna, J. A.; Soni, G. V. Fabrication of Low Noise Borosilicate Glass Nanopores for Single Molecule Sensing. *PLoS One* **2016**, *11*, No. e0157399.
(23) Madrid, E.; Rong, Y.; Carta, M.; McKeown, N. B.; Malpass-Evans, R.; Attard, G. A.; Clarke, T. J.; Taylor, S. H.; Long, Y.-T.; Marken, F. Metastable Ionic Diodes Derived from an Amine-Based Polymer of Intrinsic Microporosity. *Angew. Chem., Int. Ed.* **2014**, *53*, 10751−10754.
(24) Rong, Y.; Song, Q.; Mathwig, K.; Madrid, E.; He, D.; Niemann, R. G.; Cameron, P. J.; Dale, S. E. C.; Bending, S.; Carta, M.; Malpass-

DOI: 10.1021/acsami.9b18583
ACS Appl. Mater. Interfaces 2020, 12, 3214−3224

Evans, R.; McKeown, N. B.; Marken, F. pH-induced Reversal of Ionic Diode Polarity in 300 nm Thin Membranes Based on a Polymer of Intrinsic Microporosity. *Electrochem. Commun.* **2016**, *69*, 41−45.
(25) Aaronson, B. D. B.; Wigmore, D.; Johns, M. A.; Scott, J. L.; Polikarpov, I.; Marken, F. Cellulose Ionics: Switching Ionic Diode Responses by Surface Charge in Reconstituted Cellulose Films. *Analyst* **2017**, *142*, 3707−3714.
(26) He, D.; Madrid, E.; Aaronson, B. D. B.; Fan, L.; Doughty, J.; Mathwig, K.; Bond, A. M.; McKeown, N. B.; Marken, F. A Cationic Diode Based on Asymmetric Nafion Film Deposits. *ACS Appl. Mater. Interfaces* **2017**, *9*, 11272−11278.
(27) Tshwenya, L.; Arotiba, O.; Putra, B. R.; Madrid, E.; Mathwig, K.; Marken, F. CationicDiodes by Hot-pressing of Fumasep FKS-30 Ionomer Film onto a Microhole in Polyethylene Terephthalate (PET). *J. Electroanal. Chem.* **2018**, *815*, 114−122.
(28) Tshwenya, L.; Marken, F.; Arotiba, O. A. Carbon Nanofibers Provide a Cationic Rectifier Material: Specific Electrolyte Effects, Bipolar Reactivity, and Prospect for Desalination. *ChemElectroChem* **2019**, *6*, 3145−3153.
(29) Putra, B. R.; Harito, C.; Bavykin, D. V.; Walsh, F. C.; Wahyuni, W. T.; Boswell, J. A.; Squires, A. M.; Schmitt, J. M. F.; Da Silva, M. A.; Edler, K. J.; Fletcher, P. J.; Gesell, A. E.; Marken, F. Processes Associated with Ionic Current Rectification at a 2D-titanate Nanosheet Deposit on a Microhole Poly(ethylene terephthalate) Substrate. *J. Solid State Electrochem.* **2019**, *23*, 1237−1248.
(30) Cho, T.-H.; Tanaka, M.; Onishi, H.; Kondo, Y.; Nakamura, T.; Yamazaki, H.; Tanase, S.; Sakai, T. Battery performances and thermal stability of polyacrylonitrile nano-fiber-based nonwoven separators for Li-ion battery. *J. Power Sources* **2008**, *181*, 155−160.
(31) Godjevargova, T.; Dimov, A. Permeability and protein adsorption of modified charged acrylonitrile copolymer membranes. *J. Membr. Sci.* **1992**, *67*, 283−287.
(32) Wang, X.-l.; Wei, J.-f.; Dai, Z.; Zhao, K.-y.; Zhang, H. Preparation and characterization of negatively charged hollow fiber nanofiltration membrane by plasma-induced graft polymerization. *Desalination* **2012**, *286*, 138−144.
(33) Jain, S.; Chattopadhyay, S.; Jackeray, R.; Singh, H. Surface modification of polyacrylonitrile fiber for immobilization of antibodies and detection of analyte. *Anal. Chim. Acta* **2009**, *654*, 103−110.
(34) Yuan, H.; Wang, Y.; Yu, H.; Wei, Z.; Ge, B.; Mei, Y. Effect of UV irradiation on PAN precursor fibers and stabilization process. *J. Wuhan Univ. Technol., Mater. Sci. Ed.* **2011**, *26*, 449−454.
(35) Wu, H.; Shen, F.; Su, Y.; Chen, X.; Wan, Y. Modification of polyacrylonitrile membranes via plasma treatment followed by polydimethylsiloxane coating for recovery of ethyl acetate from aqueous solution through vacuum membrane distillation. *Sep. Purif. Technol.* **2018**, *197*, 178−188.
(36) Yue, Z.; Benak, K. R.; Wang, J.; Mangun, C. L.; Economy, J. Elucidating the porous and chemical structures of $ZnCl_2$-activated polyacrylonitrile on a fiberglass substrate. *J. Mater. Chem.* **2005**, *15*, 3142−3148.
(37) Deng, S.; Bai, R.; Chen, J. P. Behaviors and mechanisms of copper adsorption on hydrolyzed polyacrylonitrile fibers. *J. Colloid Interface Sci.* **2003**, *260*, 265−272.
(38) Bode-Aluko, C. A.; Pereao, O.; Fatoba, O.; Petrik, L. Surface-modified Polyacrylonitrile Nanofibres as Supports. *Polym. Bull.* **2017**, *74*, 2431−2442.
(39) Wang, Z.-G.; Wan, L.-S.; Xu, Z.-K. Surface engineerings of polyacrylonitrile-based asymmetric membranes towards biomedical applications: An overview. *J. Membr. Sci.* **2007**, *304*, 8−23.
(40) Kampalanonwat, P.; Supaphol, P. Preparation of Hydrolyzed Electrospun Polyacrylonitrile Fiber Mats as Chelating Substrates: A Case Study on Copper(II) Ions. *Ind. Eng. Chem. Res.* **2011**, *50*, 11912−11921.
(41) Karpacheva, G. P.; Zemtsov, L. M.; Bondarenko, G. N.; Litmanovich, A. D.; Plate, N. A. Formation of Conjugated CdN Bonds and Their Transformation in the Alkaline Hydrolysisof Poly(acrylonitrile). *Polym. Sci., Ser. A* **2000**, *42*, 620−625.
(42) Peebles, L. H.; Brandrup, J. A Chemical Means of Distinguishing between Conjugated -(1C-2C)-X and Conjugated -(C-N)-X Bonds. *Makromol. Chem.* **1966**, *98*, 189−203.
(43) Mathwig, K.; Aaronson, B. D. B.; Marken, F. Ionic Transport in Microhole Fluidic Diodes based on Asymmetric Ionomer Film Deposits. *ChemElectroChem* **2018**, *5*, 897−901.
(44) Kampalanonwat, P.; Supaphol, P. Preparation of Hydrolyzed Electrospun Polyacrylonitrile Fiber Mats as Chelating Substrates: A Case Study on Copper(II) Ions. *Ind. Eng. Chem. Res.* **2011**, *50*, 11912−11921.
(45) Bao, W.; Xu, Z.; Yang, H. Electrokinetic and permeation characterization of hydrolyzed polyacrylonitrile (PAN) hollow fiber ultrafiltration membrane. *Sci. China, Ser. B: Chem.* **2009**, *52*, 683−689.
(46) Brown, R.; Madrid, E.; Castaing, R.; Stone, J. M.; Squires, A. M.; Edler, K. J.; Takashina, K.; Marken, F. Free-Standing Phytantriol Q(224) Cubic-Phase Films: Resistivity Monitoring and Switching. *ChemElectroChem* **2017**, *4*, 1172−1180.
(47) Atkins, P. W.; De Paula, J. *Physical Chemistry*; Oxford University Press: Oxford, 2006; p 763.
(48) Nicholls, D. G.; Ferguson, S. J. *Bioenergetics*; Academic Press: Amsterdam, 2013; Vol 4, p 50.

DOI: 10.1021/acsami.9b18583
ACS Appl. Mater. Interfaces 2020, 12, 3214−3224

Electronic Supporting Information for Publication

Switching Anionic and Cationic Semi-Permeability in Partially Hydrolyzed Polyacrylonitrile: A pH-Tunable Ionic Rectifier

Luthando Tshwenya,[a] Frank Marken,[b,] Klaus Mathwig,[c] and Omotayo A. Arotiba[a,d,]**

[a] *Department of Chemical Sciences, University of Johannesburg, Doornfontein, 2028, South Africa*[1]
[b] *Department of Chemistry, University of Bath, Claverton Down, Bath BA2 7AY, UK*
[c] *The University of Groningen, Groningen Institute of Pharmacy, Pharmaceutical Analysis, P.O. Box 196, 9700 AD Groningen, The Netherlands*
[d] *Centre for Nanomaterials Science Research, University of Johannesburg, South Africa*

Corresponding author: fm202@bath.ac.uk; oarotiba@uj.ac.za

Finite element analysis

We employed COMSOL Multiphysics 5.4 to determine concentration profiles, electrical potentials and rectification by solving the Poisson-Nernst-Planck (PNP) formalism, which is also used for nanofluidic diodes [1]. We based the calculation on our previous model of rectification in asymmetric ionomer-microhole film deposits [2]. Figure S1 shows the used simulation geometry. A 13 µm high phPAN ionomer membrane is placed on a microhole with 6 µm height and 10 µm radius. The microhole and phPAN film are separated by two reservoirs of 200 µm height and 250 µm radius (the phPAN film extends across the entire radius of the upper reservoir). The outer boundaries of both reservoirs were set as constant ion concentrations (i.e., coupling to a large electrolyte reservoir). The same boundaries form electrode surfaces; the upper boundary is sweeping, while the lower is set at a constant potential of 0 V. In the PNP formalism employed here [2], analytes are transported exclusively by diffusion and migration in an electric field. This electrical field (potential distribution) is determined by the electrode potentials, by the fixed charge density in the phPAN ionomer, and by the distribution of the mobile charges of the electrolyte ions. Electroneutrality is preserved.

To achieve numerical convergence at high ionomer charge density and very steep gradients of concentrations and potentials at the ionomer boundaries, the membrane was modeled as an ion exchange membrane using Donnan boundary conditions [3] at the membrane-electrolyte interfaces.

[1] *Formerly known as the Department of Applied Chemistry, University of Johannesburg, South Africa*

For modeling the transport of the HCl electrolyte, we used bulk diffusion coefficients [4] of $D_{bulk}(H^+) = 8 \cdot 10^{-9}$ m^2/s and $D_{bulk}(Cl^-) = 2 \cdot 10^{-9}$ m^2/s.

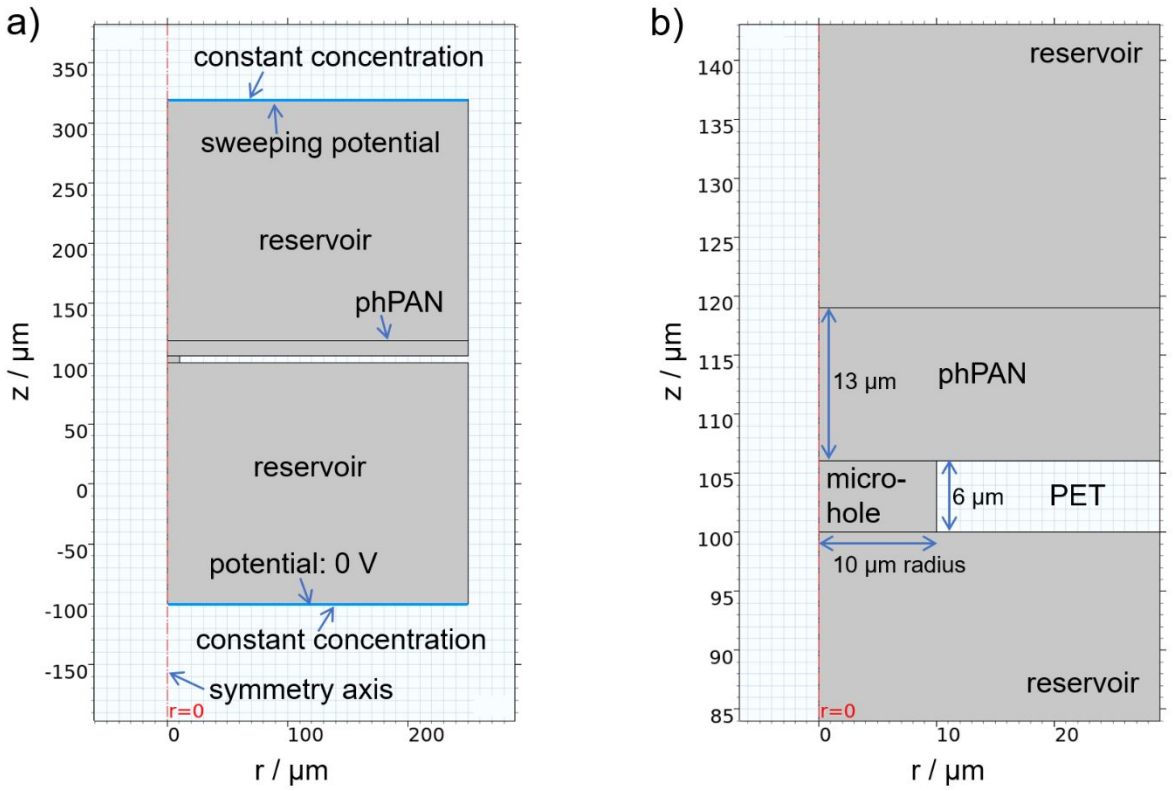

Figure S1. *Simulation geometry for numerical calculation and boundary conditions. In a two-dimensional axisymmetric geometry, the shown geometry rotates around a symmetry axis, forming two cylindrical reservoirs, a cylindrical phPAN film deposit and microhole. Panel b) zooms in on a).*

For a quantitative simulation of voltammograms, three uncertain experimental values are fitting parameters in the calculation: the density of fixed positive charges within the phPAN ionomer membrane, and the effective cation and anion diffusivities in the membrane. We chose values (without systematic fitting) of diffusion coefficients reduced to 40% compared to the bulk value, i.e., $D_{mem}(H^+,Cl) = 0.4 \cdot D_{bulk}(H^+,Cl^-)$, and a charge density of 60 mM -e^-, corresponding to 5.8 kC/dm^3.

Figure S2 shows the distributions of cations, anions the electrical potential for an open diode at a bias of -1 V at the electrode in the upper reservoir. A bulk HCl concentration of 50 mM was used. Cations and anions accumulate in the hole and phPAN film, leading to a high conductivity and a high current. The applied potential drops continuously in the hole and film.

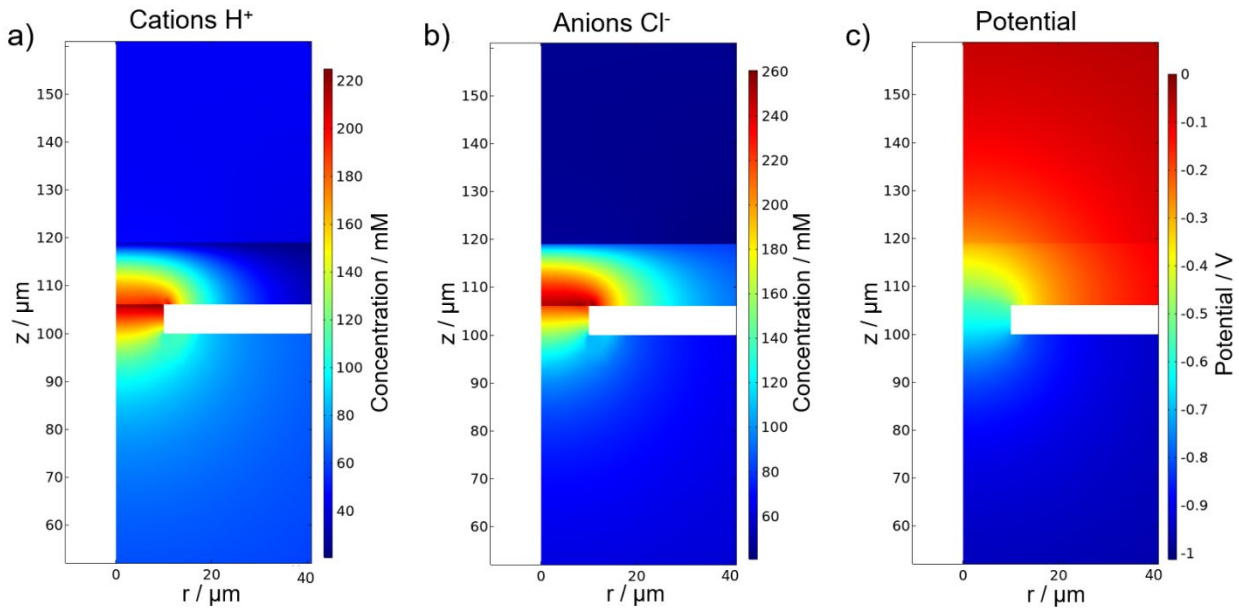

Figure S2. *Cation, anion and potential distribution in the phPAN ionomer microhole deposition in forward bias at -1 V for a 50 mM HCl concentration. The microhole is open, charge carriers accumulate in the hole and phPAN.*

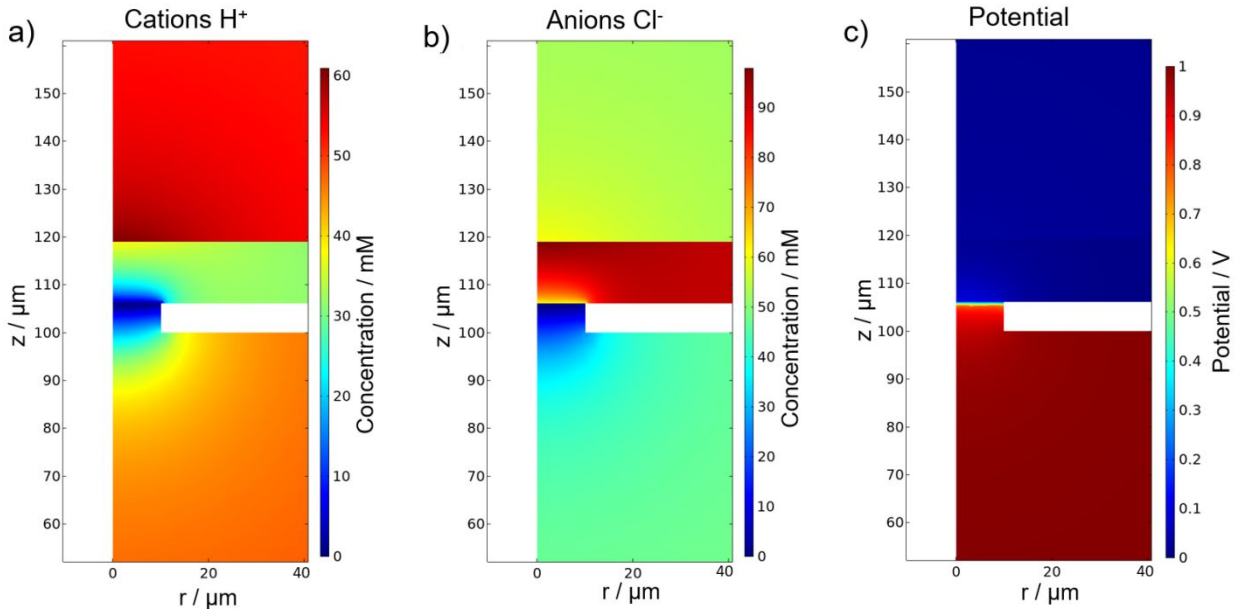

Figure S3. *Cation, anion and potential distribution in the phPAN ionomer microhole deposition in reverse bias at 1 V (50 mM bulk HCl concentration). The microhole is depleted of charge carriers.*

In Figure S3, potential and concentration profiles are shown for a blocked microhole in reversed bias at 1 V. Both cations and anions migrate out of the microhole, it is depleted of charge carriers, leading to a high resistance and small current. The charge density changes abruptly at

the phPAN-microhole interface and, thus, almost the entire applied potential drop at this interface.

For both reverse and forward bias, the concentration of Cl^- anions in the phPAN film is much higher and the H^+ concentrations. The anions compensate for the fixed positive charges in the membrane and preserved electroneutrality.

To determine currents and rectification ratios (see Figure 7 e,f in the main text), we integrated normal ion fluxes across the microhole cross section area.

Extent of hydrolysis

The degree of hydrolysis was studied by exposing polyacrylonitrile to 1 M KOH for various time periods (0 min to 25 min). Between 0 and 5 min, currents (both positive window and negative) become suppressed, but cationic diode behaviour is retained. Increasing hydrolysis time further (from 8 min to 20 min) ultimately supresses positive currents almost completely, while increasing negative currents substantially. Further than this (25 min), current starts leaking on the positive potential window and thereby decreasing diode performance. Therefore 20 minutes was chosen as the optimum time to achieve maximum/optimum diode behaviour and partial hydrolysis.

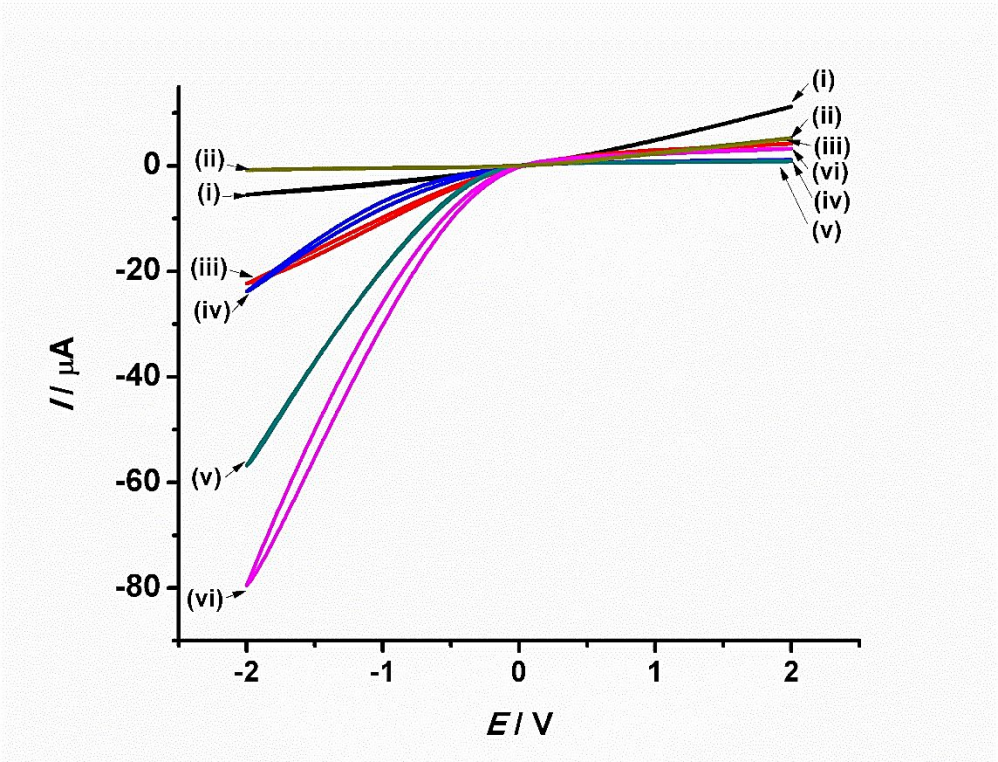

Figure S4. Cyclic voltammetry (scan rate 50 mV s^{-1}) of a polyacrylonitrile film asymmetrically covering a 20 μm diameter microhole on a PET film substrate exposed for; (i) 0 min, (ii) 5 min, (iii) 10 min, (iv) 15 min, (v) 20 min, and (vi) 25 min

References

1. Vlassiouk I, Smirnov S, Siwy Z. Nanofluidic ionic diodes. Comparison of analytical and numerical solutions. *Acs Nano* (2008) **2**:1589–1602.

2. Mathwig K, Aaronson BD, Marken F. Ionic transport in microhole fluidic diodes based on asymmetric ionomer film deposits. *ChemElectroChem* (2018) **5**:897–901.

3. How to Model Ion-Exchange Membranes and Donnan Potentials. *COMSOL Multiphysics* Available at: https://www.comsol.com/blogs/how-to-model-ion-exchange-membranes-and-donnan-potentials/ [Accessed October 3, 2019]

4. Atkins P, Paula J de, Keeler J. *Atkins' Physical Chemistry*. Eleventh Edition. Oxford, New York: Oxford University Press (2017).